

# Optimization of Retractable Structures Utilizing Bistable Compliant Mechanism

M. Ohsaki<sup>a,\*</sup>, S. Tsuda<sup>b</sup>, H. Watanabe<sup>a</sup>

<sup>a</sup>*Dept. of Architecture, Hiroshima University, Higashi-Hiroshima, Japan*

<sup>b</sup>*Dept. of Design and Technology, Okayama Prefectural University, Soja, Japan*

---

## Abstract

An optimization approach is presented for a retractable structure consisting of bistable compliant mechanism. The structure is modeled using truss and beam elements, and snapthrough behavior is utilized to generate large deformation under small input displacement and recover the initial shape by application of a small reversal force. The parameters such as nodal locations and cross-sectional areas of members are optimized to minimize the error of nodal displacements from the specified target values. It is shown that the deformed shape, required input force, and stiffness against lateral loads can be controlled independently by modifying nodal locations and stiffnesses of different sets of members. It is also shown through an example of roof model that the maximum load required for shape transformation can be effectively reduced by utilizing the flexibility and self-weight of structure.

*Keywords:* Retractable structure, Bistable compliant mechanism, Snapthrough, Optimization, Tabu search

---

---

\*Hiroshima University, 1-4-1, Kagamiyama, Higashi-Hiroshima 739-8527, Japan  
*Email address:* ohsaki@hiroshima-u.ac.jp (M. Ohsaki)

## 1. Introduction

Mechanisms are used in variety of fields of engineering including robotics and mechatronics. The direction of motion is modified and a large output displacement is generated from a small input displacement utilizing mechanisms. In order to reduce input force, it is conventional to employ an unstable bar-joint model called link mechanism. However, when an unstable mechanism is used for a retractable roof in architectural engineering, the structure cannot have required stiffness against long-term and short-term design loads. A constraining force should also be applied to ensure stability of structure in the process of shape transformation, and a force in reverse direction is needed to recover the initial shape.

Mechanisms are extensively utilized for deployable structures in architectural engineering [1, 2]. The shape of a pin-jointed truss can be controlled by placing some actuators instead of truss members. A flexible truss consisting of bars and actuators is called variable geometry truss (VGT), which is used for robot arms, deployable structures in space, etc. Senba and Furuya [3] developed an approach to optimizing the geometry of a VGT considering its vibration modes. Optimization methods for robot arms to avoid obstacles are also presented [4]. However, many actuators are generally needed for shape transformation of a VGT.

The mechanisms including VGT are also used for small deployable structures and shape transformation of long-span retractable roofs in civil and architectural engineering. However, very limited types of mechanisms such as scissors mechanism are used in this field [5, 6]. Furthermore, the parameters to realize the desired kinematic relations are adjusted manually using

explicit geometrical formulas [7, 8, 9]. Vu *et al.* [10] carried out parametric study on locations of cables and struts for deployable tension-strut structures.

In contrast to conventional unstable link mechanisms, a compliant mechanism utilizes elastic deformation of structural parts to produce large output displacement in different direction from the input displacement [11]. It can also store strain energy utilizing bistability and flexibility of the structure. In the initial definition of compliant mechanism, the structure is designed as continuum [12, 13], because it is aimed to be a single-piece product in micromechanics, and to have less frictional noise than a link mechanism. However, for large structures in civil and architectural engineering, the compliant mechanism can be modeled as a flexible bar-joint structure incorporating deformation of members. A bar-joint mechanism can be easily re-modeled to frame mechanism utilizing flexibility of joints [14, 15].

Optimization methods have been extensively developed for generating compliant mechanisms. Ohsaki and Nishiwaki [16] presented an optimization approach to generating multistable compliant bar-joint mechanisms that have multiple stable self-equilibrium states at both deformed and undeformed states utilizing snapthrough behavior and contact to an obstacle. The bar-joint structure enables us to eliminate the difficulties due to local member buckling in the optimization process considering geometrical nonlinearity. Oh and Kota [17] categorized the behaviors of bistable mechanisms. Ohsaki *et al.* [18] optimized clamping members of frame-supported membrane structures utilizing the flexibility of frame model. Huang and Xie [19] optimized a bridge-type structure considering geometrical nonlinearity.

A bistable structure that has two self-equilibrium states can also be uti-

lized to shape transformation of structures. Gantes and Konitopoulou [20] investigated constructability of a bistable deployable arch through geometrically nonlinear analysis and physical model. Keadze *et al.* [21] discussed basic properties of a bistable shell unit.

In this paper, an optimization approach is presented for designing retractable structures consisting of bistable compliant bar-joint mechanisms. Each mechanism is controlled by only single input force to generate large deformation through snapthrough behavior. Therefore, due to geometrical nonlinearity, it is not straightforward to achieve the target deformation through optimization of nodal locations and member stiffnesses. The parameters of a column-type mechanism are optimized using a heuristic approach called tabu search. It is shown that the deformed shape, required input force, and stiffness against lateral loads can be controlled independently by modifying nodal locations and stiffnesses of different sets of members. The characteristics of a roof-type bistable compliant mechanism are next compared with those of unstable link mechanism. It is shown that the maximum required force for deformation can be effectively reduced utilizing the flexibility and self-weight of structure.

## 2. Bistable compliant mechanism

In this section, we summarize, for completeness of the paper, the properties of bistable compliant mechanism modeled as a flexible bar-joint system using truss elements. Snapthrough behavior is utilized to realize a bistability of structure, which has a deformed stable self-equilibrium state in addition to the initial undeformed state; see, e.g., Refs. [16] and [22] for details.

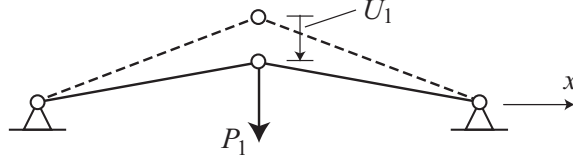


Figure 1: A two-bar truss subjected to a vertical load; dotted line: undeformed shape, solid line: deformed shape.

In order to explain the basic concept of bistability, consider a two-bar shallow truss, as shown in Fig. 1, subjected to vertical load  $P_1$ , where solid and dotted lines represent deformed and undeformed shapes, respectively. The vertical displacement of the center node is denoted by  $U_1$ .

Fig. 2(a) illustrates the sequence of deformed shapes against vertical load  $P_1$ . The thick lines denoted by ‘a’ correspond to the undeformed initial shape. We suppose that the deformation is controlled by a nodal displacement using, e.g., an actuator clamped to the node. Fig. 2(b) illustrates the relation between the input displacement  $U_1$  and the associated input force  $P_1$ . The points ‘a’, ‘b’, ..., ‘e’ in Fig. 2(b) correspond to the shapes ‘a’, ‘b’, ..., ‘e’ in Fig. 2(a), respectively. When  $U_1$  is increased from 0, the force  $P_1$  reaches the local maximum at ‘b’, which is called limit point. By further increasing  $U_1$ ,  $P_1$  reduces to 0 at ‘c’, where two bars are located horizontally between the supports. The shape ‘c’ is a self-equilibrium shape that is retained without external force. However, it is unstable if the vertical displacement is not restrained, because a slight disturbance to the node leads to a dynamic vertical displacement. By increasing  $U_1$  beyond ‘c’, the truss reaches the shape ‘d’ corresponding to an unstressed state that is reverse (reflection symmetric) to the initial shape with respect to  $x$ -axis. Obviously, this shape is stable and

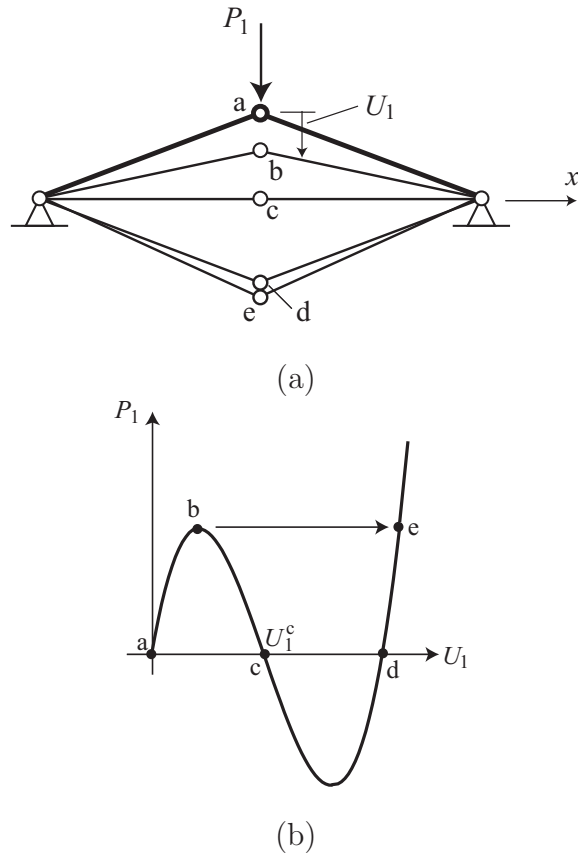


Figure 2: Relation between input force  $P_1$  and input displacement  $U_1$  of the two-bar truss exhibiting snapthrough; (a) sequence of deformed shapes; thick line: undeformed shape, thin lines: deformed shapes (b) relation between  $P_1$  and  $U_1$ .

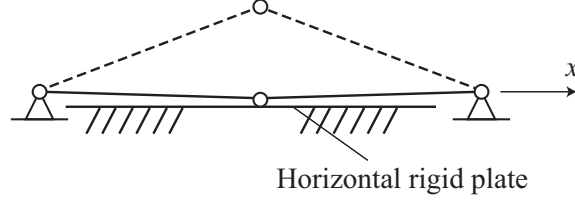


Figure 3: Termination of deformation and stabilization of the truss by contact to a horizontal rigid plate; dashed line: initial shape, solid line: deformed shape.

retained without external force.

If the deformation is controlled by the force  $P_1$ , it is possible to increase  $P_1$  stably until reaching the limit point ‘b’, where the equilibrium state jumps dynamically to ‘e’ exhibiting snapthrough. Consider the self-equilibrium point ‘c’ in Fig. 2(b) at  $U_1 = U_1^c$  satisfying  $P_1 = 0$ , and suppose a horizontal rigid plate is placed slightly below the line between the two supports, as shown in Fig. 3, to terminate the deformation slightly beyond ‘c’ and stabilize the structure by contact to the plate. A bistable mechanism with two self-equilibrium states  $U_1 = 0$  and  $U_1 \simeq U_1^c$  thus have been generated. Furthermore, the initial state can be recovered by simply adding a small upward force or disturbance at the final state. The stable unstressed state ‘d’ in Fig. 2(a) is not utilized here to generate a bistable structure, because we assign the requirement such that the initial state can be recovered by a small reverse force at the final state.

Fig. 4 illustrates a bistable compliant mechanism generating specified displacement at output node ‘B’ as a result of input displacement at node ‘A’. The properties of bistable compliant mechanism used in this paper are summarized as follows:

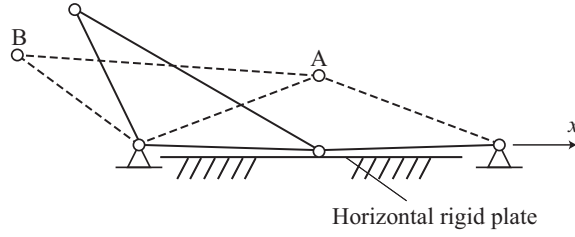


Figure 4: A bistable compliant mechanism generating specified displacement at output node B as a result of input displacement at node A; dashed line: initial shape, solid line: deformed shape.

1. A large displacement is generated at the output node in the specified direction as a result of forced displacement at the input node of the structure.
2. The deformed shape can be retained without applying external force, i.e., the structure has two self-equilibrium states including the undeformed initial state.
3. The undeformed shape can be recovered by reversely applying a small force as a disturbance to the deformed shape.

In the following examples, all members are modeled as bars (truss elements), which are pin-jointed, except the rigid parts modeled using beam elements with sufficiently large stiffness. The steel material is used for all members, where Young's modulus is 210.0 GPa and the weight density is 77.0 kN/m<sup>3</sup>. Note that the thin members are supposed to be manufactured as appropriate parts including coil springs and leaf springs.

### 3. Column-type model

#### 3.1. Definition of model

The parameters of a column-type model as shown in Fig. 5(a) is to be optimized. This model can be used for shape transformation of non-structural walls of building and long-span structures. The size of each story (square unit) is  $1 \text{ m} \times 1 \text{ m}$ . Each member is identified by the node numbers at its two ends; e.g., the member connecting nodes 1 and 2 is denoted by member 1-2. The blank and filled circles in Fig. 5(a) indicate pin and rigid joints, respectively. Note that the pin joints at nodes 13–16, respectively, actually overlap the rigid joints.

The members are classified into six groups as shown in Table 1. Groups 1 and 2 are vertical and horizontal members modeled by beam elements consisting of a box section with  $50 \times 50$  (mm) exterior square and 2.3 mm plate thickness; accordingly, the cross-sectional area is  $4.388 \times 10^{-4} \text{ m}^2$ . The pairs of members (12-13,13-7), (13-14,14-8), (14-15,15-9), (15-16,16-10), and (16-17,17-11) are connected rigidly at nodes 13, 14, 15, 16, and 17, respectively, whereas members 13-14, 14-15, 15-16, and 16-17 are pin-jointed to nodes 13, 14, 15, and 16, respectively.

All other members are modeled by truss elements; accordingly, nodes  $1, \dots, 12$  and  $18, \dots, 22$  are pin joints. The vertical truss members 6-18, 18-7,  $\dots$ , 22-11 in the right side of the column and member 12-6 between the supports are classified into group 3, and have the same cross-sectional area  $4.388 \times 10^{-4} \text{ m}^2$  as the beam members in groups 1 and 2. The remaining truss members have very small cross-sectional areas; hence, these members are actually manufactured as springs with the same extensional stiffnesses as

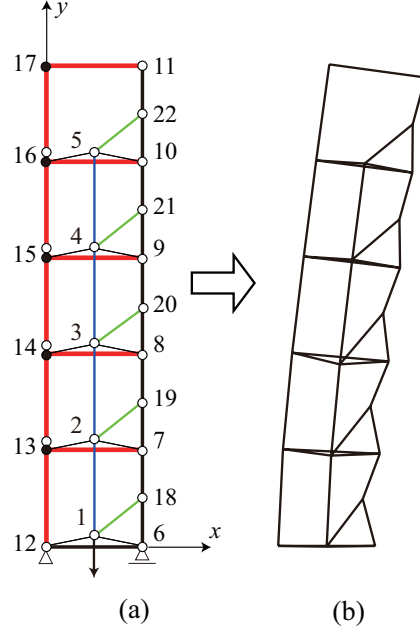


Figure 5: A column-type model; (a) geometry and node numbers; blank circle: pin joint, filled circle: rigid joint, (b) illustration of deformed shape in real scale.

Table 1: Member sections of column model;  $\square$ : box section.

Group	Members	Section
1	12-13, 13-14, 14-15, 15-16, 16-17	beam: $\square - 50 \times 50 \times 2.3$
2	13-7, 14-8, 15-9, 16-2, 17-11	beam: $\square - 50 \times 50 \times 2.3$
3	6-18, 18-7, 7-19, 19-8, 8-20, 20-9 9-21, 21-10, 10-22, 22-11, 12-6	truss: $A = 4.388 \times 10^{-4} \text{ m}^2$
4	1-2, 2-3, 3-4, 4-5	truss: $A = \text{variables}$
5	12-1, 1-6, 13-2, 2-7, 14-3 3-8, 15-4, 4-9, 16-5, 5-10	truss: $A = 1.0 \times 10^{-6} \text{ m}^2$
6	1-18, 2-19, 3-20, 4-21, 5-22	truss: $A = 1.0 \times 10^{-6} \text{ m}^2$

the truss members. Note that the weights of thin truss members do not have much effect on the total weight.

The vertical displacement applied at node 1 is transmitted to nodes 2, 3, 4, and 5 by the vertical members in group 4. Note that the members in group 4 are not connected to the horizontal members in group 2. The symmetrically located diagonal thin members, which are classified into group 5, are compressed to generate snapthrough behavior, and the vertical displacements of nodes 1, 2, 3, 4, and 5 are transformed by the diagonal members in the right-hand-side, which are classified into group 6, to lateral displacements of nodes 18, 19, 20, 21, and 22. Consequently, the deformation as shown in Fig. 5(b) is generated.

### *3.2. Optimization problem*

A general purpose frame analysis software OpenSees Ver. 2.3.2 [23] is used for geometrically nonlinear analysis against vertical forced displacement at node 1. The absolute value of reaction force first increases and reaches a limit point, and decreases to 0 to generate the deformed shape in Fig. 5(b). The final shape is defined such that the reaction force first reaches 0 after undergoing snapthrough behavior as illustrated as point ‘c’ in Fig. 2(b). The geometry and stiffness of the mechanism is optimized to minimize the deviation of the final shape from the specified target shape. In this process, we ignore deformation against self-weight and additional lateral loads to be considered in real-world design, and confirm the behavior of the optimized mechanism under practical design loads in the following section.

Although the structure remains in elastic range, the displacements at the final state cannot be obtained within an accuracy required to apply a

gradient-based nonlinear programming approach, because the deformation is geometrically nonlinear and the final state is to be approximated by interpolation between consecutive two steps of incremental analysis. Therefore, we use a heuristic approach called tabu search for optimization, which is summarized in Appendix.

Let  $x_1, \dots, x_m$  denote the  $m$  real design variables that are discretized into integer variables  $J_i \in \{1, \dots, s_i\}$  ( $i = 1, \dots, m$ ), which means that  $J_i$  can take an integer value between 1 and  $s_i$ . The upper and lower bounds of  $x_i$  are denoted by  $x_i^U$  and  $x_i^L$ , respectively. Then, the relation between  $x_i$  and  $J_i$  is given as

$$x_i = x_i^L + \frac{J_i - 1}{s_i - 1}(x_i^U - x_i^L), \quad (i = 1, \dots, m) \quad (1)$$

Therefore, all properties of the mechanism are functions of the integer variable vector  $\mathbf{J} = (J_1, \dots, J_m)$ .

We minimize the mean deviation  $E(\mathbf{J})$  between the specified displacement components at the final state from the target values. Let  $\mathbf{U}$  and  $\mathbf{U}^*$  denote the vector of specified  $q$  displacement components and their target values, respectively. The optimization problem is formulated, as follows, as an unconstrained problem:

$$\text{Minimize } E(\mathbf{J}) = \left( \frac{1}{q} \|\mathbf{U}(\mathbf{J}) - \mathbf{U}^*\| \right)^{\frac{1}{2}} \quad (2a)$$

$$\text{subject to } J_i \in \{1, \dots, s_i\}, \quad (i = 1, 2, \dots, m) \quad (2b)$$

The design variables in the following examples are the cross-sectional areas  $A_{1-2}$ ,  $A_{2-3}$ ,  $A_{3-4}$ ,  $A_{4-5}$  of four members in group 4 and the  $y$ -coordinates  $Y_1, \dots, Y_5$  of nodes  $1, \dots, 5$ ; i.e., we have nine design variables.

Table 2: Target and optimal values of lateral displacements (m) of nodes 8–11.

Node		8	9	10	11
Opt-1	Target value	0.120	0.260	0.420	0.500
	Optimal value	0.1411	0.2588	0.3851	0.5189
Opt-2	Target value	0.150	0.325	0.525	0.625
	Optimal value	0.1742	0.3240	0.4842	0.6515
Opt-3	Target value	0.18	0.39	0.63	0.750
	Optimal value	0.2280	0.3878	0.5640	0.7525

Table 3: Lower and upper bounds of variables for Opt-1, Opt-2, and Opt-3.

	Opt-1		Opt-2, 3	
	Lower	Upper	Lower	Upper
$A_{1-2}$ (m <sup>2</sup> )	$5.0 \times 10^{-7}$	$5.0 \times 10^{-6}$	$2.0 \times 10^{-6}$	$7.0 \times 10^{-6}$
$A_{2-3}$ (m <sup>2</sup> )	$5.0 \times 10^{-7}$	$5.0 \times 10^{-6}$	$2.0 \times 10^{-6}$	$7.0 \times 10^{-6}$
$A_{3-4}$ (m <sup>2</sup> )	$5.0 \times 10^{-7}$	$5.0 \times 10^{-6}$	$2.0 \times 10^{-6}$	$7.0 \times 10^{-6}$
$A_{4-5}$ (m <sup>2</sup> )	$5.0 \times 10^{-7}$	$5.0 \times 10^{-6}$	$5.0 \times 10^{-6}$	$1.5 \times 10^{-5}$
$Y_1$ (m)	0.05	0.15	0.10	0.20
$Y_2$ (m)	1.05	1.15	1.10	1.20
$Y_3$ (m)	2.00	2.10	1.95	2.05
$Y_4$ (m)	3.00	3.10	2.95	3.05
$Y_5$ (m)	4.00	4.10	3.95	4.05

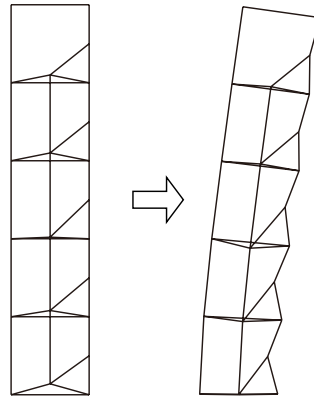
Table 4: Optimal solutions of column-type model.

	Opt-1	Opt-2	Opt-3
$A_{1-2} (\times 10^{-6} \text{m}^2)$	5.00	7.00	3.00
$A_{2-3} (\times 10^{-6} \text{m}^2)$	0.95	6.00	5.50
$A_{3-4} (\times 10^{-6} \text{m}^2)$	0.50	2.50	3.00
$A_{4-5} (\times 10^{-6} \text{m}^2)$	1.00	5.00	6.00
$Y_1$ (m)	0.14	0.13	0.16
$Y_2$ (m)	1.08	1.10	1.11
$Y_3$ (m)	2.02	2.03	2.03
$Y_4$ (m)	3.10	2.95	2.95
$Y_5$ (m)	4.10	3.95	3.95
Objective function (m)	0.02249	0.02951	0.03147
$U_1^y$ (m)	-0.147	-0.1521	-0.168

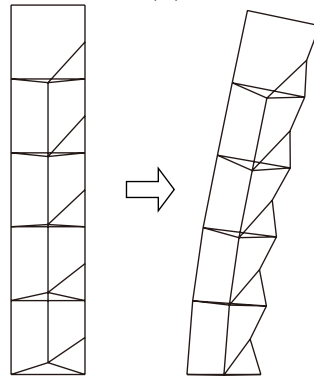
### 3.3. Optimization results

Optimization is carried out for three cases designated as Opt-1, Opt-2, and Opt-3, for which the target  $x$ -directional displacements of nodes 8, 9, 10, and 11 are given in Table 2. The bounds of variables for Opt-1, Opt-2, and Opt-3 are listed in Table 3.

Tabu search is carried out from five different random seeds, and the best solution among the five trials is selected as the optimal solution. The number  $s_i$  of discrete values is 11 for all variables. For example, for the variable  $Y_1$  of Opt-1, integer values  $1, 2, \dots, 11$  correspond to real values  $0.05, 0.06, \dots, 0.15$  (m), respectively. We assume, from the manufacturing point of view, the



(a)



(b)

Figure 6: Initial and final shapes of optimal solutions; (a) Opt-1, (b) Opt-3.

increment 0.01 m is sufficiently small. For TS, the number of neighborhood solutions is 18, the number of steps is 200, and the length of tabu list is 2000. The optimal solutions are listed in Table 4. The lateral displacements are also listed in Table 2. Although the displacements of nodes 8 and 10 do not have good agreement with the target values, those of nodes 9 and 11 are close to their target values, and the optimal objective values in Table 4 are sufficiently small. The maximum relative errors for Opt-1, Opt-2, and Opt-3 are 17.6%, 16.1%, and 26.7%, respectively. We confirmed through a random search of the optimal solutions using real values that the errors are not due to discretization and we cannot adjust the displacements completely to the target value by modifying a limited number of variables. The configurations of Opt-1 and Opt-3 are shown in Fig. 6(a) and (b), respectively, where the left figures are initial shapes, and the right figures are final shapes. The objective value and the vertical displacement  $U_1^y$  of node 1 at the final state are also listed in Table 4 for each optimal solution. The optimal solution Opt-1, which has the smallest objective value among the three solutions, is hereafter called ‘standard model’, and its properties are investigated under practical design loads.

Note again that the thin members are actually manufactured as springs. For example, for member 1-12 of the standard model, the cross-sectional area modeled as a truss member is  $A = 1.0 \times 10^{-6} \text{ m}^2$ , Young’s modulus is 210 GPa, and the initial and final lengths are 0.519 m and 0.5 m, respectively. Therefore, the extensional stiffness is 404 N/mm, if it is modeled as a spring. It has been confirmed that the deformation and stiffness of the spring are within practically admissible ranges.

Quasi-static analysis is carried out for the optimized mechanism using a finite element analysis software package ABAQUS Ver. 6.10 [24]. Let  $G$  denote the acceleration of gravity. The analysis consists of the following three steps with respect to time  $t$ :

**Step 1:**  $0 \leq t \leq 1$ : Application of vertical gravity load of  $1.0G$  to all members without fixing node 1.

**Step 2:**  $1 \leq t \leq 2$ : Shape transformation under forced vertical displacement at node 1 to the final value  $U_1^y$  listed in Table 4.

**Step 3:**  $2 \leq t \leq 3$ : Application of lateral load of  $0.2G$  to all members in positive  $x$ -direction after constraining vertical displacement of node 1.

The solid line in Fig. 7 shows variation of vertical reaction force  $R_1^y$  at node 1 with respect to time  $t$  of the standard model. A snapthrough behavior is observed in negative  $y$ -direction, and the maximum absolute value of reaction force is 2.641 kN. In the following, the maximum value  $R_1^{y(\max)}$  is assumed to represent the maximum absolute value, for brevity. Note that the reaction force at the final state of shape transformation ( $t = 2.0$ ) has a rather large value 0.570 kN due to gravity load that is not incorporated in the optimization process; however, if we stop the process at the self-equilibrium state without reaction force, which is slightly before  $t = 2$ , then only a small upward force is needed to recover the initial state.

The lateral displacement  $U_{11}^x$  of node 11 is plotted in Fig. 8. The values of  $R_1^{y(\max)}$ , as well as the values of  $R_1^y$  and  $U_{11}^x$  at  $t = 2$  and 3 are summarized as ‘Standard’ in Table 5. The relative displacements during shape transformation ( $1 \leq t \leq 2$ ) and those against lateral loads ( $2 \leq t \leq 3$ ) are

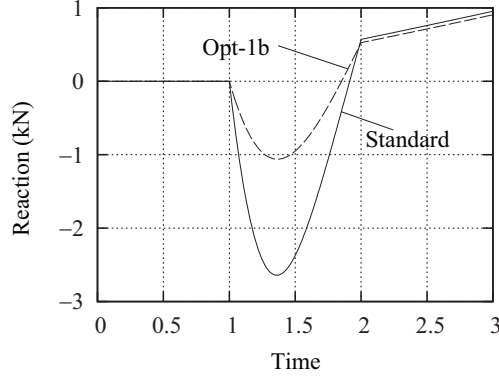


Figure 7: Vertical reaction force  $R_1^y$  of node 1; solid line: standard model, dashed line: Opt-1b.

denoted by superscripts (S) and (L), respectively; i.e.,  $U_{11}^{x(S)} = 0.5435$  m and  $U_{11}^{x(L)} = 0.5703 - 0.5435 = 0.0268$  m. The value of  $U_{11}^{x(L)}$  is also listed in Table 5. Note that  $U_{11}^{x(L)}$  of the standard model is larger than 0.025 m that is equivalent to 1/200 of the total height 5.0 m. The required vertical load  $R_1^y$  and the stiffness against lateral loads can be independently modified as follows.

If we increase the cross-sectional area  $A_6^g$  of the members in group 6 to the five times of the standard model,  $U_{11}^{x(S)}$  and  $U_{11}^{x(L)}$  become 0.5309 m and 0.0230 m, respectively, while  $R_1^{y(max)}$  is 2.649 kN as summarized as Opt-1a in Table 5. This way, the displacement due to lateral loads can be reduced effectively without increasing the maximum reaction force.

Let  $A_6^{g*}$  denote the ratio of  $A_6^g$  to the value of the standard model. The ratios of other values are also indicated by superscript \*. Variations of  $R_1^{y(max)*}$ ,  $U_{11}^{x(S)*}$ , and  $U_{11}^{x(L)*}$  are plotted with respect to  $A_6^{g*}$  in Fig. 9, which confirms that  $R_1^{y(max)*}$  is almost constant with respect to  $A_6^{g*}$ .

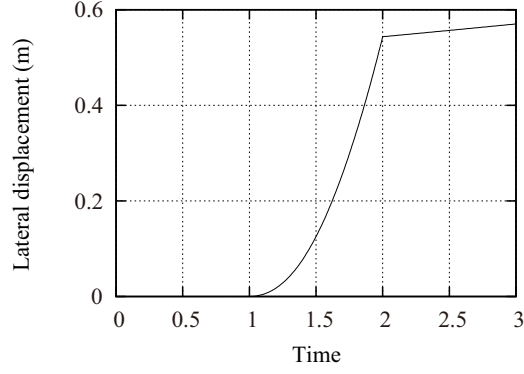


Figure 8: Lateral displacement  $U_{11}^x$  of node 11 of standard model.

Table 5: Maximum reaction force  $R_1^{y(\max)}$  (kN), and values of reaction force  $R_1^y$  (kN) and lateral displacements  $U_{11}^x$  (m) of node 11 at  $t = 2$  and 3, and  $U_{11}^{x(L)}$  (m) of column-type model.

		$R_1^{y(\max)}$	$t = 2$	$t = 3$	$U_{11}^{x(L)}$
Standard	Displacement	–	0.5435	0.5703	0.0268
	Reaction	2.641	0.5701	0.9529	–
Opt-1a	Displacement	–	0.5309	0.5539	0.0230
	Reaction	2.649	0.5450	0.9158	–
Opt-1b	Displacement	–	0.4796	0.5192	0.0396
	Reaction	1.061	0.5258	0.9053	–

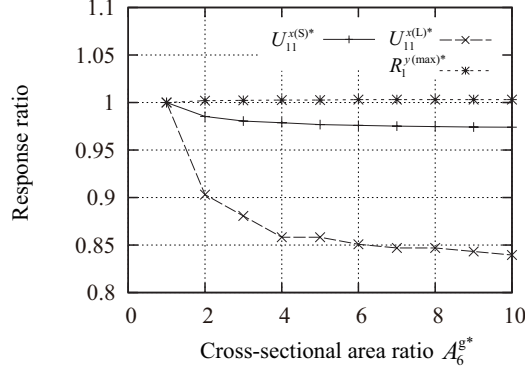


Figure 9: Variations of ratios of reaction forces and displacements with respect to ratio of cross-sectional area of group 6; solid line:  $U_{11}^{x(S)*}$ , dashed line:  $U_{11}^{x(L)*}$ , dotted line:  $R_1^{y(max)*}$ .

If we decrease the cross-sectional area  $A_5^g$  of members in group 5, which is directly related to snapthrough behavior, to half of the standard model, then the reaction force becomes as shown in the dashed line in Fig. 7. This model is designated as Opt-1b. The maximum reaction force  $R_1^{y(max)}$  is 1.061 kN, which is less than half of the standard model. The values of  $U_{11}^{x(S)}$  and  $U_{11}^{x(L)}$  are 0.4796 m and 0.0396 m, respectively, as summarized as Opt-1b in Table 5; i.e., Opt-1b has less reaction force  $R_1^{y(max)}$  but larger displacement  $U_{11}^{x(L)}$  than Opt-1a. Therefore, the cross-sectional areas can be decided in view of trade-off between reaction force and displacements. Variations of  $R_1^{y(max)*}$ ,  $U_{11}^{x(S)*}$ , and  $U_{11}^{x(L)*}$  are plotted with respect to  $A_5^{g*}$  in Fig. 10, which confirms that  $U_{11}^{x(S)*}$  and  $U_{11}^{x(L)*}$  are almost constant with respect to  $A_5^{g*}$ . The maximum absolute value of stress in the truss and beam members except the thin members are 41.66, 40.74, and 29.75 (MPa), for standard model (Opt1), Opt1-a, and Opt1-b, respectively, all of which are in the beam connecting

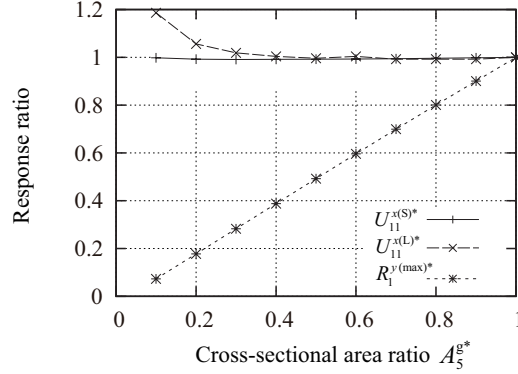


Figure 10: Variations of ratios of reaction forces and displacements with respect to ratio of cross-sectional area of group 5; solid line:  $U_{11}^{x(S)*}$ , dashed line:  $U_{11}^{x(L)*}$ , dotted line:  $R_1^{y(max)*}$ .

nodes 8 and 14. The maximum stress does not depend on the cross-sectional areas of thin members in group 6; however, it depends on those of group 5. Since deformation of a compliant mechanism is concentrated in the restricted parts, which are manufactured as springs, the stresses of the remaining members are sufficiently small; i.e., the maximum stresses for three cases are less than 1/7 of the yield stress of a steel material, and stress of a beam member can be reduced if its cross-sectional property is modified without changing the self-weight.

If we do not consider the gravity for Opt1-b, the variation of  $R_1^y$  becomes as plotted in the solid line in Fig. 11, which is to be compared with the dashed line with gravity. As is seen, the maximum reaction force can be reduced utilizing the self-weight of the structure.

The results in this section reveal that utilization of flexibility, or equivalently, stiffness of the structure has several advantages over unstable mecha-

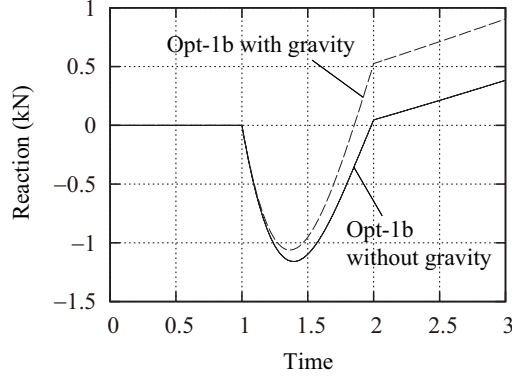


Figure 11: Vertical reaction force  $R_1^y$  of node 1 of column-type model; solid line: Opt-1b without gravity, dashed line: Opt-1b with gravity.

nisms, which are summarized as follows:

1. The structure in the process of shape transformation can be stabilized by constraining only the vertical input displacement; i.e., lateral constraint is not needed.
2. Only one actuator is needed to generate global shape transformation.
3. Only downward force is needed for shape transformation, because the initial state can be recovered by application of small upward force at the final state, if we stop the process slightly beyond the first self-equilibrium state that appears after reduction of reaction force from the limit point.
4. The structure after constraining single node at the final state has enough stiffness against lateral loads.
5. The required input force and stiffness against lateral loads can be controlled independently by modifying stiffnesses of different sets of members.

Table 6: Nodal coordinates (m) of roof models 1 and 2.

Node	Model 1	Model 2
1	(0,2.5,2.5)	(0,2.93,0)
2	(0,0,0)	(0,0,0)
3	(0,0,3)	(0,0,3)
4	(0,10,5)	(0,10,5.7115)
5	(5,5,0)	(5,5,0)
6	(−5,5,0)	(−5,5,0)
7	(0,5,0)	—

Note that the plane mechanisms obtained here can easily be converted to 3-dimensional mechanisms with hexahedral units. The buckling triangular parts are extended to tetrahedral parts. We have confirmed this re-modeling; however, the result is not presented here, because it is rather obvious.

#### 4. Roof model

The purpose of this section is to investigate the effectiveness of utilizing flexibility and geometrical nonlinearity of structure using the roof model as shown in Fig. 12, which is designated as model 1. Geometrically nonlinear analysis quasi-static analysis is carried out using ABAQUS.

Let  $(X_i, Y_i, Z_i)$  denote the coordinates of the  $i$ th node, which are listed in Table 6. Boundary conditions are given to preserve symmetry with respect to  $yz$ -plane. Nodes 1, 2, 3, and 7 are fixed in  $x$ -direction, node 2 is fixed in  $y$ -direction, and nodes 2, 5, 6, and 7 are fixed in  $z$ -direction. All members

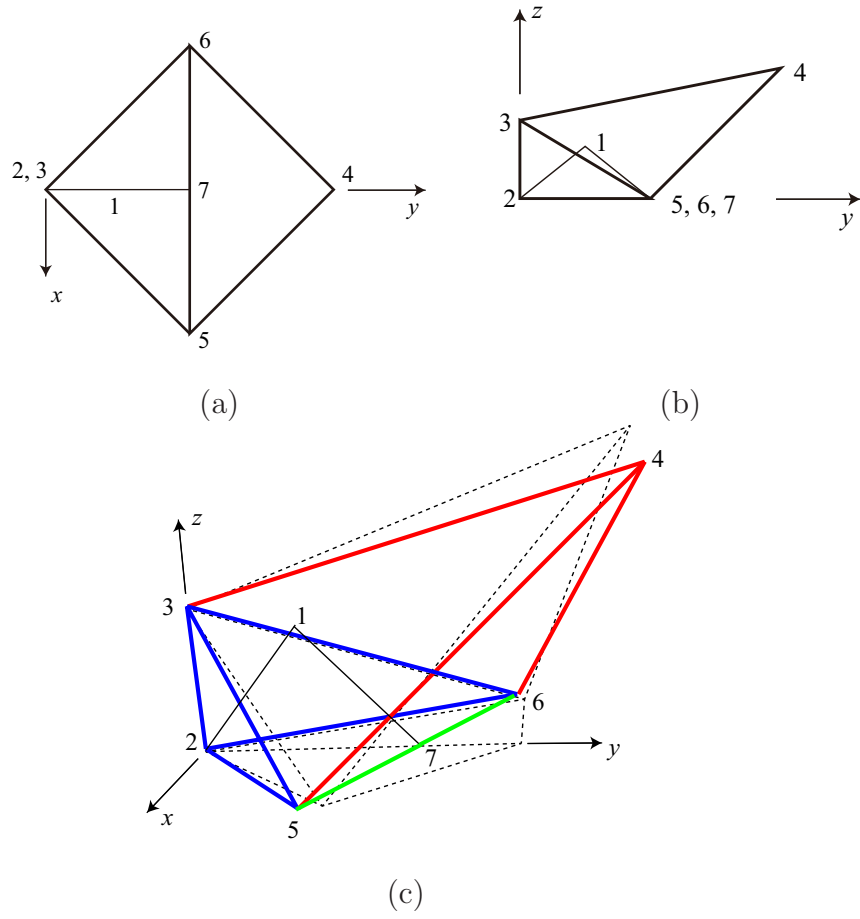


Figure 12: Roof model 1; (a) plan, (b) elevation, (c) diagonal view; solid line: initial shape, dotted line: deformed shape.

except the flexible member are modeled as truss element with the cross-sectional area  $0.02194 \text{ m}^2$ , which is sufficiently large so as to concentrate the deformation at the flexible member. The triangular planes 2-3-5 and 2-3-6 represent the walls, and the roof consists of triangular planes 4-3-5 and 4-3-6. By application of forced downward displacement at node 1, node 7 moves in  $x$ -direction, and the distance between nodes 5 and 6 decreases; consequently, the top node 4 moves upward. A vertical load  $25.0 \text{ kN}$  and a lateral load  $5.0 \text{ kN}$ , respectively, are given at node 4 in addition to the gravity load of  $1.0G$  and the horizontal load of  $0.2G$ , where the vertical load is estimated from the covering area and the load per unit area of the roof. The same loading history is given as the column-type model; i.e., gravity is applied in the period  $0 \leq t \leq 1$ , shape transformation is carried out in  $1 \leq t \leq 2$ , and lateral load in  $y$ -direction is applied in  $2 \leq t \leq 3$ .

This model, called model 1-1, is unstable before fixing node 1, which is pulled down to the  $xy$ -plane to move node 4 upward from  $Z_4 = 5.0$  to  $5.7115$  (m). The  $z$ -directional reaction force  $R_1^z$  of node 1 is plotted in solid line in Fig. 13. Note that  $R_1^z$  at the final state of shape transformation ( $t = 2$ ) corresponds to the weight of members 1-2 and 1-7, which are collinear on  $xy$ -plane.

Next we consider a compliant model, called model 1-2, that has a thin member with cross-sectional area  $2.194 \times 10^{-7} \text{ m}^2$  between nodes 2 and 7. Note that the cross sectional area is  $1/100000$  of that of the stiff members. This structure is stable without fixing node 1. The thin member is to be manufactured as a spring with extensional stiffness  $9.215 \text{ N/mm}$ , which is sufficiently small as a practically available coil spring.

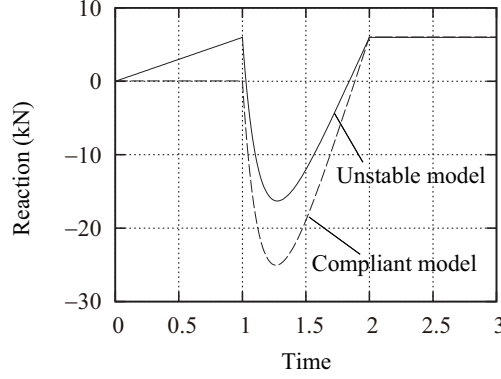


Figure 13: Reaction force  $R_1^z$  of node 1 of model 1; solid line: unstable model 1-1, dashed line: compliant model 1-2.

Let  $\mathbf{U}_i = (U_i^x, U_i^y, U_i^z)$  denote the displacement vector of node  $i$ . The displacements (m) of nodes 4, 5, and 6 at  $t = 1$  due to self-weight and vertical load, which are simply denoted as self-weight for brevity, are sufficiently small. The reaction force  $R_1^z$  of model 1-2 is plotted in dashed line in Fig. 13, which indicates that the maximum absolute value of  $R_1^z$  becomes larger if we assign a thin member. However, because  $R_1^z$  at the final state is positive, this state can be stabilized easily by assigning an obstacle slightly below  $xy$ -plane to terminate deformation beyond the self-equilibrium state before  $t = 2$ . Hence, the initial state can be recovered by applying a small upward force. The maximum absolute value of stress in the truss members is 12.36 MPa, which is about 1/25 of the yield stress of a steel material.

We next consider roof model 2 as shown in Fig. 14, which is unstable, and a pair of members 1-5 and 1-6 are located on  $xy$ -plane. The boundary conditions are the same as model 1 except node 1 that is fixed in  $x$ - and  $z$ -directions. This model is designated as model 2-1. If we pull node 1 in

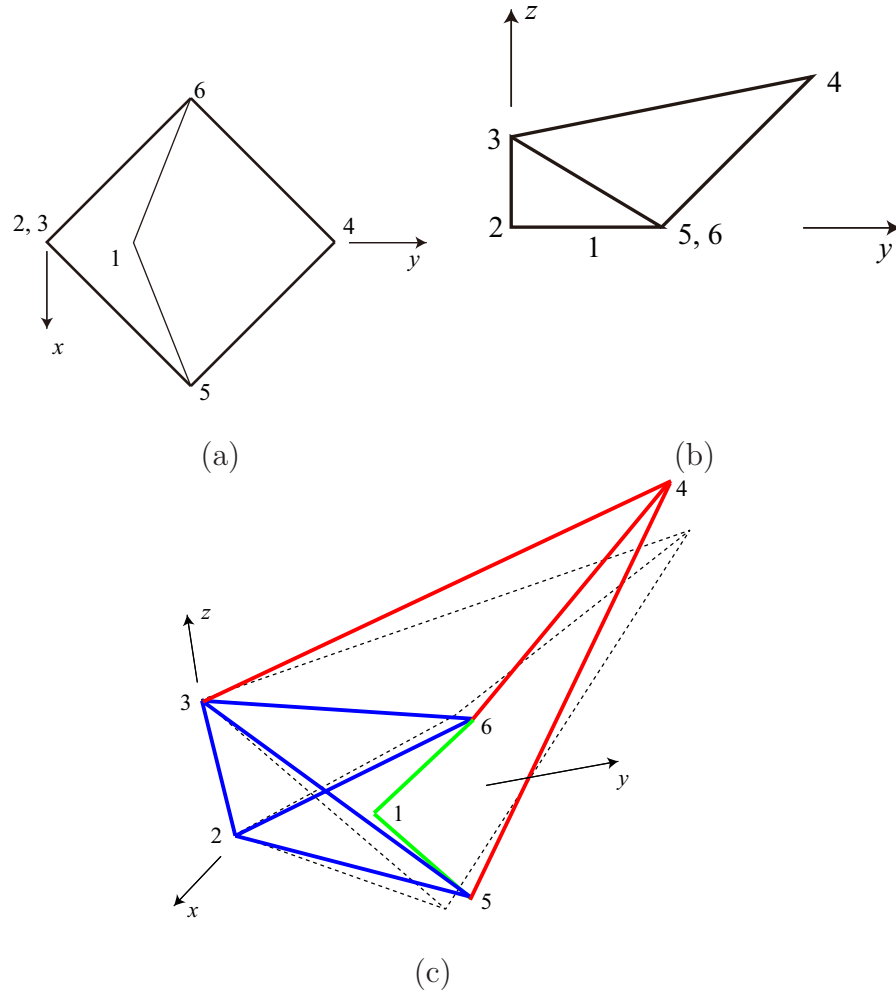


Figure 14: Roof model 2; (a) plan, (b) elevation, (c) diagonal view; solid line: initial shape, dotted line: deformed shape.

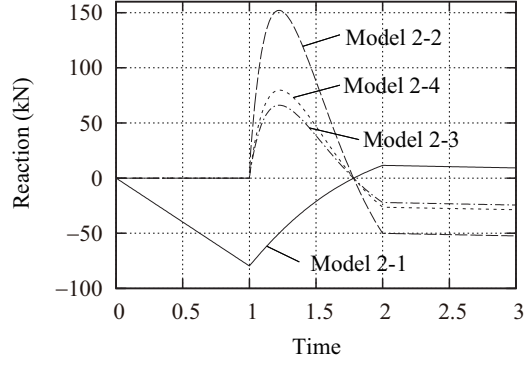


Figure 15: Reaction force  $R_1^y$  of node 1 of roof model 2; solid line: model 2-1 (unstable), dashed line: model 2-2 (compliant), chain line: model 2-3 (small spring), dotted line: model 2-4 (without self-weight of model 2-3).

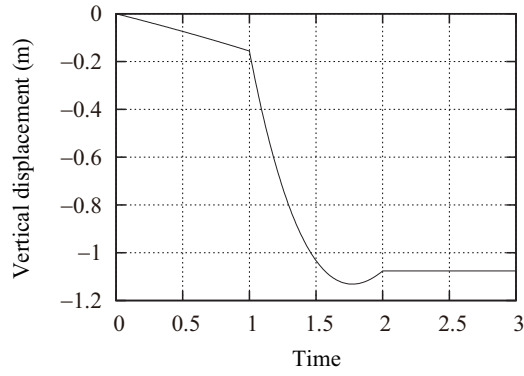


Figure 16: Vertical displacement  $U_4^z$  of node 4 of roof model 2-3.

$y$ -direction on  $xy$ -plane, then the distance between nodes 5 and 6 increases; consequently, the top node 4 moves downward, which is opposite to model 1-1, to the shape shown in dotted lines in Fig. 14. Since  $Z_4 = 5.7115$  at the final state after shape transformation of model 1-1, the initial shape of model 2-1 is given as  $Z_4 = 5.7115$  to demonstrate the reverse process. The  $y$ -directional reaction  $R_1^y$  of node 1 is plotted in solid line in Fig. 15, which shows that  $R_1^y$  is larger than  $|R_1^z|$  of model 1-1.

A thin member is next placed between nodes 5 and 6 to stabilize the mechanism. Let  $A_s$  denote the cross-sectional area of the thin member. For Model 2-2,  $A_s = 2.194 \times 10^{-5} \text{ m}^2$  that is equivalent to a spring with extensional stiffness 460.7 N/mm, which is in a practical range. Note that the cross sectional area is 1/1000 of that of the stiff members. For this model, the  $z$ -directional displacement  $U_4^z$  of node 4 at  $t = 1$  is  $-0.2757 \text{ m}$ . All nodal displacements at  $t = 1$  are compensated to update the initial shape to obtain the reaction force as plotted in dashed line in Fig. 15, which shows that the maximum absolute value of reaction, denoted by  $R_1^{y(\max)}$ , increases as a result of adding a thin member. Therefore, we decrease  $A_s$  to  $1.097 \times 10^{-5} \text{ m}^2$ , which is called model 2-3, to obtain the chain line in Fig. 15 that has less  $R_1^{y(\max)}$  than the unstable model 2-1. Note that the cross sectional area is 1/2000 of that of the stiff members. Furthermore, it is important to note that no reaction force is needed at node 1 at  $t = 1$ . Variation of  $U_4^z$  is plotted with respect to  $t$  in Fig. 16. The displacement at  $t = 1$  is  $0.1558 \text{ m}$ , which can be reduced if we allow larger reaction force. Alternatively, the initial location of node 4 may be adjusted so that it is placed at the desired location at  $t = 1$ . The maximum absolute value of stress in the truss members is 5.17 MPa in

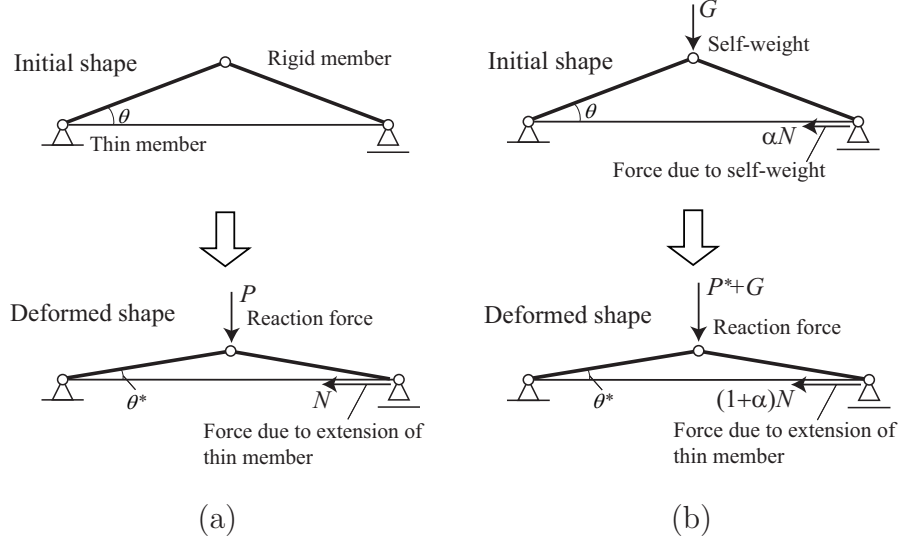


Figure 17: Illustration of effect of self-weight on reaction force of a two-bar truss; (a) deformation without self-weight, (b) deformation with self-weight.

the members connecting nodes 2 and 5, and 2 and 6. Note that the value is about 1/60 of the yield stress of a steel material.

By contrast, if we consider model 2-4 without the self-weight for model 2-3,  $R_1^y$  becomes as plotted in dotted line in Fig. 15. Therefore, the maximum reaction force can be reduced by incorporating the self-weight.

Fig. 17 illustrates the reduction of reaction force for a forced deformation due to self-weight of a symmetric two-bar truss. The inclination angle of the rigid bars decreases from  $\theta$  at the undeformed initial state to  $\theta^*$  at a deformed state, as shown in Fig. 17(a), where the reaction force and axial force of the thin member are  $P$  and  $N$ , respectively; i.e.,

$$P = 2N \tan \theta^* \quad (3)$$

Fig. 17(b) illustrates the same deformation considering self-weight. The un-

stressed state is adjusted so that the angle is  $\theta$  after application of self-weight  $G$ . The axial force of the thin member at this state is denoted by  $\alpha N$ . Assuming linearity between axial force and axial deformation of the thin member, the increase of axial force from the initial state to the deformed state with the angle  $\theta^*$  has the same value  $N$  as the case without self-weight; i.e., the axial force at the deformed state is  $(1 + \alpha)N$ , where the reaction force is denoted by  $P^*$ .

Define  $\beta$  by

$$\beta = \frac{\tan \theta^*}{\tan \theta} \quad (4)$$

which is less than 1. Then, the axial force  $N^*$  of the thin member in equilibrium with the self-weight, excluding  $P^*$ , after deformation is found as

$$\begin{aligned} N^* &= \frac{G}{2 \tan \theta^*} \\ &= \frac{G}{2 \beta \tan \theta} \\ &= \frac{\alpha N}{\beta} \\ &> \alpha N \end{aligned} \quad (5)$$

Hence, the axial force in equilibrium with the self-weight increases due to deformation. The reaction force  $P^*$  is written as

$$\begin{aligned} P^* &= 2(1 + \alpha)N \tan \theta^* - G \\ &= 2(1 + \alpha)N \tan \theta^* - 2\alpha N \tan \theta \\ &= 2 \left( 1 + \alpha - \frac{\alpha}{\beta} \right) N \tan \theta^* \\ &= P + 2\alpha \left( 1 - \frac{1}{\beta} \right) N \tan \theta^* \\ &< P \end{aligned} \quad (6)$$

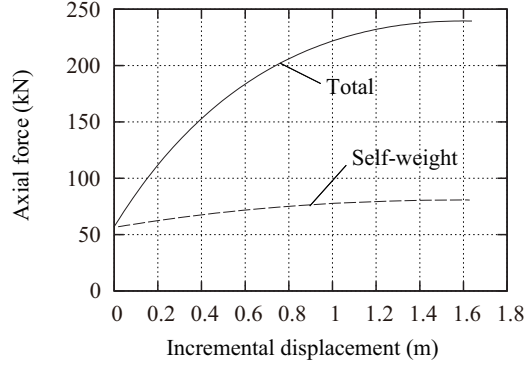


Figure 18: Relation between  $\Delta U_1^y$  and axial force of thin member 5-6 of model 2-3; solid line: total axial force, dashed line: axial force due to self-weight.

This way, the reaction force decreases due to existence of self-weight, if the contribution of self-weight on the axial force increases.

In order to investigate more details of this property for model 2-3, the axial force  $N_{5-6}$  of thin member 5-6 of model 2-3 is plotted with respect to  $U_1^y$  in Fig. 18. The solid line shows the relation between the incremental displacement  $\Delta U_1^y$  from  $t = 1$  and  $N_{5-6}$  for  $1 \leq t \leq 2$  of model 2-3, and the dashed line is the value of  $N_{5-6}$ , denoted by  $N_{5-6}^0$ , that satisfies equilibrium against the self-weight without reaction force  $R_1^y$ . Therefore,  $N_{5-6} - N_{5-6}^0$  corresponds to the axial force due to forced displacement  $\Delta U_1^y$ . Note that the axial forces of members connected to nodes 5 and 6 also have effect on the axial forces of members 1-5 and 1-6, and accordingly, on  $R_1^y$ ; hence, the overall properties can be characterized by the axial force of member 5-6 that directly correspond to the snapthrough behavior. As seen from Fig. 18,  $R_1^y$  decreases owing to the self-weight, because  $N_{5-6}^0$  is an increasing function of  $U_1^y$ , which means that the contribution of self-weight increases as deformation

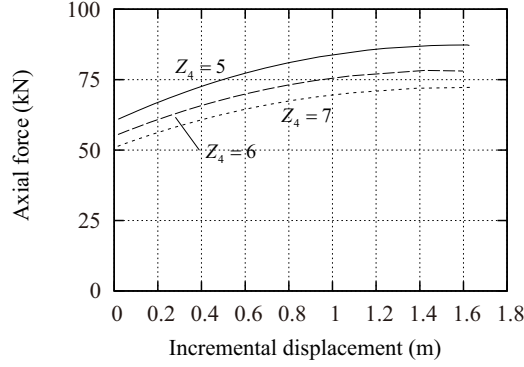


Figure 19: Relation between  $\Delta U_1^y$  and axial force  $N_{5-6}^0$  of thin member 5-6 due to self-weight for various initial height  $Z_4$  of model 2-3; solid line:  $Z_4 = 5$  m, dashed line:  $Z_4 = 6$  m, dotted line  $Z_4 = 7$  m.

proceeds. Fig. 19 shows the relation between  $U_1^y$  and  $N_{5-6}^0$  for various initial height  $Z_4 = 5, 6$ , and  $7$  m of model 2-3. Note that  $N_{5-6}^0$  is an increasing function of  $U_1^y$  for all cases, and a smaller height leads to a larger axial force. This way, the self-weight may be effectively utilized to reduce the maximum force needed for shape transformation of a shallow roof.

## 5. Conclusions

An optimization approach has been presented for designing retractable structures utilizing bistable compliant mechanisms exhibiting snapthrough behavior. The parameters, including nodal coordinates and member cross-sectional areas, of a column-type mechanism are optimized to realize target deformation using a heuristic approach called tabu search. The properties of the optimized column-type mechanism have been extensively investigated through geometrically nonlinear analysis considering self-weight and lateral

design load. It is important to note that the required input force and stiffness against lateral loads can be controlled independently by modifying stiffnesses of different sets of members.

The characteristics of roof-type bistable compliant mechanism have also been compared with those of unstable link mechanisms. It has been shown that the maximum load for shape transformation can be reduced utilizing the flexibility of the mechanism and self-weight of the structure. This property has been clearly demonstrated through a simple example of a two-bar truss.

## References

- [1] Gantes CJ, Connor JJ, Logcher RD, Rosenfield Y. Structural analysis and design of deployable structures. *Comput Struct* 1989;32:661–669.
- [2] Gantes CJ. *Deployable structures: Analysis and design*. WIT Press; 2001.
- [3] Senba A, Furuya H. Optimal configuration for the self-identification of a two-dimensional variable geometry truss. *Struct Multidisc Optim* 2010;40:453–465.
- [4] Agirrebeitia J, Avilés R, de Bustos IF, Ajuria G. Inverse position problem in highly redundant multibody systems in environments with obstacles. *Mechanism and Machine Theory* 2003;38:1215–1235.
- [5] Thrall AP, Adriaenssens S, Paya-Zaforteza I, Zoli TP. Linkage-based movable bridges: Design methodology and three novel forms. *Eng Struct* 2012;37:214–223.

- [6] Akgün Y, Gantes CJ, Sobek W, Korkmaz K, Kalochairetis K. A novel adaptive spatial scissor-hinge structural mechanism for convertible roofs. *Eng Struct* 2011;33:1365–1376.
- [7] Akgün Y, Gantes CJ, Kalochairetis KE, Kiper G. A novel concept of convertible roofs with high transformability consisting of planar scissor-hinge structures. *Eng Struct* 2010;32:2873–2883.
- [8] Pellegrino S. Deployable structures. Springer;2002.
- [9] Karni E, Pellegrino S. A retractable small-span roof based on thin-walled lightweight spatial units. *Int J Space Struct* 2007;22(2):93–106.
- [10] Vu KK, Liew JYR, Anandasivam K. Deployable tension-strut structures: From concept to implementation. *J Constr Steel Res* 2006;62:195–209.
- [11] Howell LL, Compliant mechanisms. Wiley;2001.
- [12] Bruns TE, Tortorelli DA. Topology optimization of non-linear structures and compliant mechanisms. *Comput Methods Appl Mech Engrg* 2001;190:3443–3459.
- [13] Sigmund O. On the design of compliant mechanisms using topology optimization. *Mech Struct & Mach* 1997;25(4):493–524.
- [14] Ramrakhyami DS, Frecker MI, Lesieutre GA. Hinged beam elements for the topology design of compliant mechanisms using the ground structure approach. *Struct Multidisc Optim* 2009;37:557–567.

- [15] Kinoshita Y, Ohsaki M. Synthesis of bistable compliant structures from truss mechanism. *J Computational Science and Technology JSME* 2009;3(2):417–425.
- [16] Ohsaki M, Nishiwaki S. Shape design of pin-jointed multistable compliant mechanism using snapthrough behavior. *Struct Multidisc Optim* 2005;30:327–334.
- [17] Oh YS, Kota S. Synthesis of multistable equilibrium compliant mechanisms using combinations of bistable mechanisms. *J Mech Design* 2009;131:Paper.021001.
- [18] Ohsaki M, Nakajima T, Fujiwara J, Takeda F. Configuration optimization of clamping members of frame-supported membrane structures. *Eng Struct* 2011;33:3620–3627.
- [19] Huang X, Xie YM. Topology optimization of nonlinear structures under displacement loading. *Eng Struct* 2008;30:2057–2068.
- [20] Gantes CJ, Konitopoulou E. Geometric design of arbitrary curved bistable deployable arches with discrete joint size. *Int J Solids Struct* 2004;41:5517–5540.
- [21] Kebabze E, Guest SD, Pellegrino S. Bistable prestressed shell structures. *Int J Solids Struct* 2004;41:2801–2820.
- [22] Jensen BD, Howell LL. Bistable configuration of compliant mechanisms modeled using four links and translational joints. *J Mech Eng* 2004;126(7):657–666.

- [23] PEERC, Open system for earthquake engineering simulation (OpenSees), UCB, CA, 2006, (available at <http://opensees.berkeley.edu/>).
- [24] ABAQUS Ver. 6.10.3 Documentation. SIMULIA. 2011.

## Appendix

Algorithm of tabu search is summarized as follows:

- Step 1** Randomly generate a seed solution  $\hat{\mathbf{J}}$ , and initialize the tabu list  $T$  as  $T = \{\hat{\mathbf{J}}\}$ . Evaluate the objective function and initialize the incumbent optimal objective value as  $F^{\text{opt}} = F(\hat{\mathbf{J}})$ .
- Step 2** Generate a set of  $q$  neighborhood solutions  $N = \{\mathbf{J}_1^N, \dots, \mathbf{J}_q^N\}$  from  $\hat{\mathbf{J}}$ , and evaluate the objective value of each solution.
- Step 3** Among the solutions in the set  $N$ , select the best one that has the maximum value of  $F(\mathbf{J}_j^N)$ , and is not included in the list  $T$ . Assign the best solution as the new seed solution  $\hat{\mathbf{J}}$ .
- Step 4** Update the incumbent optimal objective value as  $F^{\text{opt}} = F(\hat{\mathbf{J}})$ , if  $F(\hat{\mathbf{J}}) > F^{\text{opt}}$ .
- Step 5** Add  $\hat{\mathbf{J}}$  to the list  $T$ . Remove the oldest solution from  $T$ , if the number of solutions in  $T$  exceeds the specified limit.
- Step 6** Output  $F^{\text{opt}}$  and the corresponding optimal solution, if the number of iterations reaches the specified value; otherwise, go to Step 2.